




Article

High-Temperature Spin Crossover in Iron(II) Complexes with 2,6-Bis(1*H*-imidazol-2-yl)pyridine

Ludmila G. Lavrenova ^{1,*}, Olga G. Shakirova ^{1,2,*}, Evgeniy V. Korotaev ¹, Svetlana V. Trubina ¹,
Alexsei Ya. Tikhonov ³, Irina A. Os'kina ³, Sergey A. Petrov ⁴, Konstantin Yu. Zhizhin ⁵, and
Nikolay T. Kuznetsov ⁵

- ¹ Nikolaev Institute of Inorganic Chemistry, Siberian Branch, Russian Academy of Sciences, Academic Lavrentyev Avenue 3, 630090 Novosibirsk, Russia
- ² Department of Chemistry and Chemical Technologies, Faculty of Machinery and Chemical Technologies, Federal State Budget Institution of Higher Education, Komsomolsk-na-Amure State University, Lenin Avenue 27, 681013 Komsomolsk-on-Amur, Russia
- ³ N.N. Vorozhtsov Novosibirsk Institute of Organic Chemistry Siberian Branch, Russian Academy of Sciences, Academic Lavrentyev Avenue 9, 630090 Novosibirsk, Russia
- ⁴ Institute of Solid State Chemistry, Siberian Branch, Russian Academy of Sciences, Kutateladze Street 18, 630128 Novosibirsk, Russia
- ⁵ Kurnakov Institute of General and Inorganic Chemistry, Russian Academy of Sciences, Leninskii Avenue 31, 119991 Moscow, Russia
- * Correspondence: ludm@niic.nsc.ru (L.G.L.); shakirova_olga@mail.ru (O.G.S.)

Abstract: Novel iron(II) coordination compounds containing a ligand 2,6-bis(1*H*-imidazol-2-yl)pyridine (L), having such a composition as [FeL₂]SO₄·0.5H₂O, [FeL₂]Br₂·H₂O, [FeL₂](ReO₄)₂, [FeL₂]B₁₀H₁₀·H₂O, [FeL₂]B₁₂H₁₂·1.5H₂O had been synthesized and studied using UV-Vis (diffuse reflectance), infrared, extended X-ray absorption fine structure (EXAFS), and Mössbauer spectroscopy methods, as well as X-ray diffraction and static magnetic susceptibility methods. The analysis of the $\mu_{\text{eff}}(T)$ dependence in the temperature range of 80–600 K have shown that all the obtained complexes exhibit a high-temperature spin crossover $^1A_1 \leftrightarrow ^5T_2$.

Keywords: iron(II) complexes; 2,6-bis(1*H*-imidazol-2-yl)pyridine; X-ray diffraction analysis; EXAFS; Mössbauer; IR; UV-Vis (diffuse reflectance) spectroscopy methods; spin crossover



Citation: Lavrenova, L.G.; Shakirova, O.G.; Korotaev, E.V.; Trubina, S.V.; Tikhonov, A.Y.; Os'kina, I.A.; Petrov, S.A.; Zhizhin, K.Y.; Kuznetsov, N.T. High-Temperature Spin Crossover in Iron(II) Complexes with 2,6-Bis(1*H*-imidazol-2-yl)pyridine. *Molecules* **2022**, *27*, 5093. <https://doi.org/10.3390/molecules27165093>

Academic Editor: Carlo Santini

Received: 29 June 2022

Accepted: 5 August 2022

Published: 10 August 2022

Publisher's Note: MDPI stays neutral with regard to jurisdictional claims in published maps and institutional affiliations.



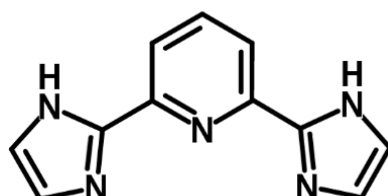
Copyright: © 2022 by the authors. Licensee MDPI, Basel, Switzerland. This article is an open access article distributed under the terms and conditions of the Creative Commons Attribution (CC BY) license (<https://creativecommons.org/licenses/by/4.0/>).

1. Introduction

Searching for novel coordination compounds wherein the spin state of the central atom can be switched by an external action is an urgent problem. This is indicated by regularly appearing publications in the literature devoted to this topic [1–8]. These compounds include iron(II) complexes with spin crossover (SCO) $^1A_1 \leftrightarrow ^5T_2$. The change in spin multiplicity occurs owing to affecting temperature, pressure, irradiation with light of a certain wavelength (LIESST effect), high-frequency magnetic or electric field, and other factors. The transition from a low-spin (LS) to a high-spin (HS) state causes a change in the magnetic, optical, and vibrational properties of the complexes. An important property associated with the spin transition consists in changing metal–donor interatomic distance amounting to 0.2 Å in the case of Fe(II) complexes. Owing to the universal properties of complexes with SCO they have a wide range of potential applications in making optoelectronic, molecular electronic, and spintronic devices [9–15]. At present, polyfunctional materials combining SCO and other properties are under active study [16–19].

2,6-Bis(1*H*-imidazol-2-yl)pyridines represent a promising class of potential ligands for the synthesis of complexes with SCO [20]. Earlier, we have reported the studies on iron(II) complexes with 2,6-bis(benzimidazol-2-yl)- and 2,6-bis(4,5-dimethyl-1*H*-imidazol-2-yl)pyridine [21–24], wherein SCO is exhibited. It seemed worthwhile to continue these

investigations into synthesizing and studying Fe(II) complexes with 2,6-bis(1*H*-imidazol-2-yl)pyridine (Scheme 1), which does not contain substituents at the imidazole fragment. Earlier, this ligand was used in order to synthesize complexes with Ru(II), and with a number of metals belonging to the first transition series [25–29]. The X-ray diffraction data have shown that L is coordinated to the metal ion in a tridentate-cyclic manner by two nitrogen atoms belonging to two imidazole rings and one nitrogen atom belonging to pyridine.



Scheme 1. 2,6-Bis(1*H*-imidazol-2-yl)pyridine (L).

2. Materials and Methods

2.1. Materials

Commercial metal salts and solvents without further purification were used in the synthesis. 2,6-Bis(imidazol-2-yl)pyridine was synthesized as described in [30] (NMR spectra of ligand given in the Supplementary Materials, Figures S1–S4); $K_2B_{10}H_{10} \cdot 2H_2O$, $K_2B_{12}H_{12}$ were obtained according to the procedure [31].

2.2. Synthesis of $[FeL_2]SO_4 \cdot 0.5H_2O$ (**1**·**0.5H₂O**)

A 0.28 g (1 mmol) sample of $FeSO_4 \cdot 7H_2O$ with the addition of 0.1 g of ascorbic acid was dissolved in 10 mL of water under heating; a 0.51 g (2 mmol) L was dissolved in 10 mL of ethanol, and the solutions were then heated and mixed. The resulting solution was evaporated until a red-violet precipitate began to form. After the solution with the precipitate was cooled in a crystallizer with ice, the precipitate was filtered off, washed twice with small portions of water, and dried in air. Yield: 55%. Anal. Calc. for $C_{22}H_{19}FeN_{10}O_{9/2}S$, (583.4): C, 45.3; H, 3.3; N, 24.0. Found: C, 46.2; H, 3.5; N, 23.4.

2.3. Synthesis of $[FeL_2]Br_2 \cdot H_2O$ (**2**·**H₂O**) and $[FeL_2](ReO_4)_2$ (**3**)

A 0.28 g (1 mmol) sample of $FeSO_4 \cdot 7H_2O$ was dissolved in 5 mL of distilled water acidified with 0.1 g of ascorbic acid. An excess (0.43 g, 1.5 mmol) of $KReO_4$ or KBr (0.36 g, 3 mmol) in 10 mL of water and a solution of L (0.51 g, 2 mmol) in 10 mL of ethanol were successively added to the resulting solution under stirring. The resulting solution was evaporated until a red-violet precipitate began to form. After the solution with the precipitate was cooled in a crystallizer with ice, the precipitate was filtered off, washed twice with small portions of water, and dried in air. Yield: 70% (**2**·**H₂O**), 30% (**3**). Anal. Calc. for $C_{22}H_{20}Br_2FeN_{10}O$, (656.1): C, 40.3; H, 3.1; N, 21.3. Found: C, 41.3; H, 3.2; N, 21.0. Anal. Calc. for $C_{22}H_{18}FeN_{10}O_8Re_2$, (978.7): C, 27.0; H, 1.9; N, 14.3. Found: C, 27.5; H, 2.2; N, 14.6.

2.4. Synthesis of $[FeL_2]B_{10}H_{10} \cdot H_2O$ (**4**·**H₂O**) and $[FeL_2]B_{12}H_{12} \cdot 1.5H_2O$ (**5**·**1.5H₂O**)

A 0.14 g (0.5 mmol) sample of $FeSO_4 \cdot 7H_2O$ was dissolved in 3 mL of distilled water acidified with 0.05 g of ascorbic acid. An excess (0.23 g, 1 mmol) of $K_2B_{10}H_{10} \cdot 2H_2O$ or $K_2B_{12}H_{12}$ (0.22 g, 1 mmol) in 10 mL of water and a solution of L (0.21 g, 1 mmol) in 5 mL of ethanol were added to the resulting solution under stirring. Red-brown precipitates began to form immediately. Each precipitate was filtered off, washed twice with small portions of water and ethanol, and dried in air. Yield: 45% (**4**·**H₂O**), 68% (**5**·**1.5H₂O**). Anal. Calc. for $C_{22}H_{30}B_{10}FeN_{10}O$, (614.5): C, 43.0; H, 4.9; N, 22.8. Found: C, 42.5; H, 5.0; N, 22.1. Anal. Calc. for $C_{22}H_{33}B_{12}FeN_{10}O_{3/2}$, (647.1): C, 40.8; H, 5.1; N, 21.6. Found: C, 40.6; H, 5.3; N, 20.9.

2.5. Measurement and Characterization

The data for elemental analysis of the complexes was acquired on a EURO EA 3000 analyzer (EuroVector, Pavia, Italy).

X-ray absorption spectra (XAS) in the Fe K edge region (150 eV before and 800 eV after) were measured in the transmission mode with the use of synchrotron radiation on the 8 beamline, VEPP-3 storage ring at the Siberian Synchrotron and Terahertz Radiation Center (Budker Institute of Nuclear Physics, Siberian Branch, Russian Academy of Sciences, Novosibirsk, Russia) [32]. A Si(111) cut-off crystal was used as a two-crystal monochromator. The operating mode of the storage ring during measurement: energy—2 GeV; current—70–140 mA. For measurements, the samples were mixed with cellulose powder as a filler and pressed into tablets. The mass of the sample was calculated so that the absorption jump at the Fe K-edge was 0.8–1. The preprocessing of the absorption spectra (selection of the oscillating part—EXAFS spectra) was performed with the use of the VIPER 10.17 program [33]. The “radial pair distribution function” (Figure 1) was obtained by the Fourier transform of the k^3 -weighted EXAFS function in the range of wave vectors $k = 2.0$ – 11.0 \AA^{-1} .

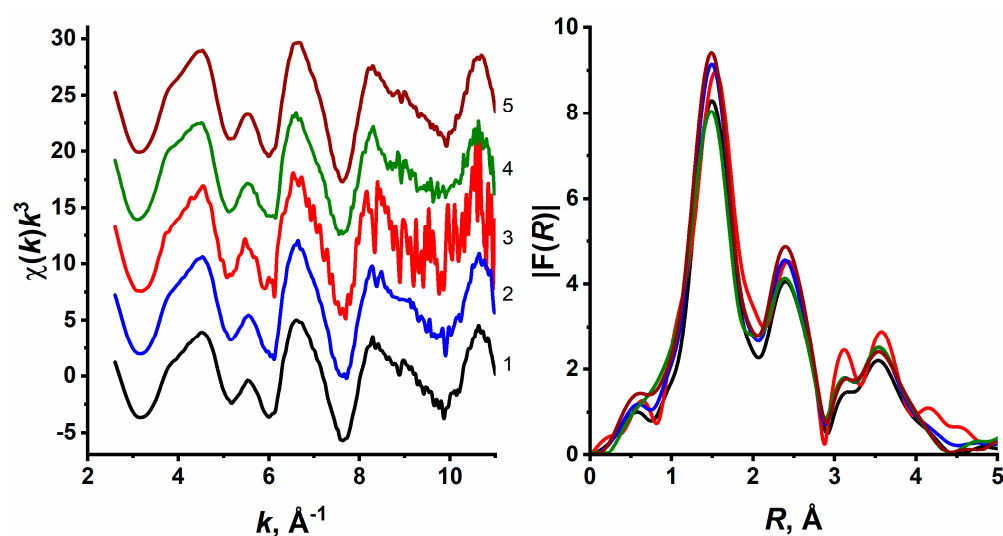


Figure 1. Fe K-edge EXAFS spectra (left) and their Fourier transform modules without consideration of the phase shift (right) of complexes 1–5.

The local environment of the Fe ion [interatomic distances (R_i) and angles (Q_i), coordination numbers (N_i), and Debye–Waller factors (σ^2)] was modeled using the EXCURVE 98 cod [34]. In this program phase and amplitude characteristics were calculated in the von-Bart and Hedin approximation. The amplitude suppression factor S_0^2 due to multielectron processes was determined for the crystallographically characterized compound ($S_0^2 = 0.85$) and fixed during further modeling of the studied compounds spectra. The Debye–Waller factor was the same separately for nitrogen and carbon atoms.

IR spectra were taken on a Scimitar FTS 2000 in the range of 4000 – 400 cm^{-1} and a Vertex 80 in the range of 600 – 100 cm^{-1} . Compound samples were prepared as suspensions in vaseline and fluorinated oils and in polyethylene.

The Kubelka–Munk diffuse reflectance spectra were obtained on a Shimadzu UV-3101 PC scanning spectrometer.

The XRD investigation of polycrystalline samples was performed using a Shimadzu XRD 7000 diffractometer ($\text{CuK}\alpha$ radiation).

The static magnetic susceptibility was measured using Faraday balance type setup equipped with electromagnetic compensating torsion quartz microbalance. The Delta DTB9696 temperature controller (Delta Electronics Inc., Taipei, Taiwan) was used for the investigated compounds temperature stabilization ($\sim 1 \text{ K}$) in the range of temperatures

80–600 K. The temperature scanning rate for the process of heating or cooling samples was ~1 K/min. The magnetic field strength (7300 Oe) stabilization precision was ~2%. The compounds studied were sealed in quartz cellules filled with atmospheric air at 760 Torr. In order to study the effect of crystallization water, the samples were placed in open quartz ampoules and vacuumed at 10^{-2} Torr, after which the helium atmosphere at 5 Torr was formed.

The effective magnetic moment of studied compounds was calculated as:

$$\mu_{eff} = \left(\frac{3k}{N_A \mu_B^2} \cdot \chi T \right)^{1/2} \approx (8\chi T)^{1/2},$$

k —Boltzmann constant, N_A —Avogadro constant, and μ_B —Bohr magneton. In the above formula, the diamagnetic contribution in total magnetic susceptibility (χ) was taken into account using the method of Pascal's constants. The direct ($T_{c\uparrow}$) and reverse ($T_{c\downarrow}$) transitions temperatures were obtained using condition the magnetic moment second derivative zero value ($d^2(\mu_{eff}(T))/dT^2 = 0$).

The Mössbauer spectra were collected with a spectrometer NP-610 (KFKI, Budapest, Hungary), using ^{57}Co in a metal Rh matrix as a radioactive source. The spectra were measured at a room temperature. The spectra were processed to find the values of isomer shift δ and quadrupole splitting ε . The isomer shifts are given relative to metal iron.

3. Results and Discussion

Iron(II) complexes with 2,6-bis(1*H*-imidazol-2-yl)pyridine were isolated from aqueous-ethanol solutions. To maintain the oxidation state of iron(II), ascorbic acid was added to the solution.

Complex **1**·0.5H₂O was synthesized by reacting stoichiometric amounts of FeSO₄ and L. Syntheses **2**·H₂O, **3**, **4**·H₂O, **5**·1.5H₂O were carried out in two stages. At the first stage, the corresponding iron(II) salts were obtained by adding a 1.5- or 2-fold excess of KBr, KReO₄, K₂B₁₀H₁₀ or K₂B₁₂H₁₂ into a solution of FeSO₄ salt. At the second stage, a solution of the ligand in ethanol was added to the resulting salt solution. The obtained diffraction patterns show that the synthesized compounds are crystalline, while [FeL₂](SO₄)·0.5H₂O and [FeL₂]Br₂·H₂O, as well as [FeL₂]B₁₀H₁₀·H₂O and [FeL₂]B₁₂H₁₂·1.5H₂O are isotypical.

The structure of the whole molecule for all complexes in the LS state ($T = 297$ °C) was established from the EXAFS data using the multiple scattering approximation within the software package EXCURV (except for [FeL₂](ReO₄)₂ (**3**)) excluding hydrogen atoms, and anions that exert only a weak effect on the shape of the EXAFS spectrum owing to their spatial separation from the central iron ion. For complex **3**, the signal-to-noise ratio in the EXAFS spectrum is worse than that for the spectra of other complexes owing to the presence of a heavy anion ReO₄[−]. Simulation of the whole molecule in the multiple scattering approximation gives too large errors in determining the parameters. Therefore, the simulation of the EXAFS spectrum for complex **3** could be carried out only in a single scattering approximation. The structure of the complexes in the LS state (by the example of complex **4**·H₂O) obtained by means of EXAFS spectra simulation is presented in Figure 2.

Table 1 lists the microstructure parameters of the coordination site for complexes **1**·0.5H₂O, **2**·H₂O, **4**·H₂O, **5**·1.5H₂O.

The structure of the coordination site of complex [FeL₂](ReO₄)₂ (**3**) in the LS state was obtained from modeling the spectrum filtered in real space ($\Delta R = 0.9$ to 3.0 Å). The simulation data are presented in Table 2. The coordination numbers of the nearest spheres of the iron ion environment were fixed in accordance with the data obtained in the simulation of complexes in the LS state in the multiple scattering approximation.

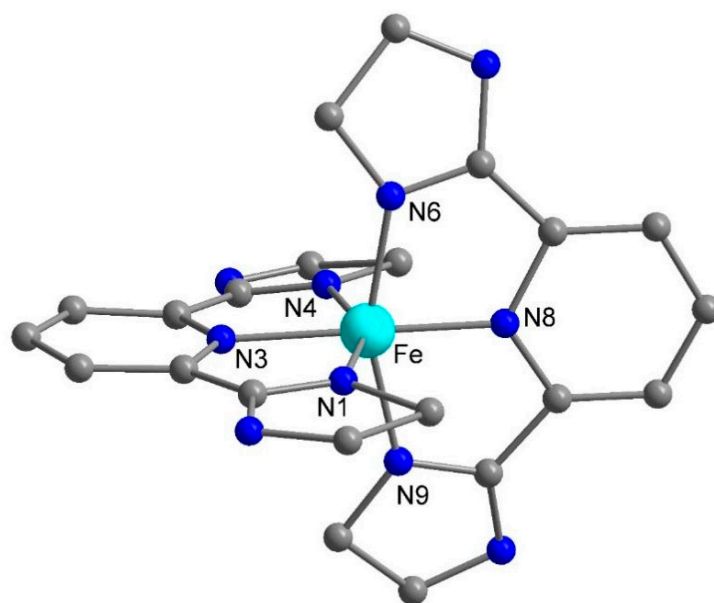


Figure 2. General view of the structure of the coordination core obtained by means of EXAFS spectra simulation for such complexes as $1 \cdot 0.5\text{H}_2\text{O}$, $2 \cdot \text{H}_2\text{O}$, $4 \cdot \text{H}_2\text{O}$, $5 \cdot 1.5\text{H}_2\text{O}$.

Table 1. Microstructure parameters of the Fe coordination site for the complexes at $T = 300 \text{ K}$ (LS) obtained by EXAFS fitting with multiple scattering approximation (R_i —interatomic distance, $2\sigma_i^2$ —Debye–Waller factor, F_i —the statistical error of the fitting).

Bonds	$R_i, \text{Å}$				Angles	$\Omega, \text{Deg.}$			
	$1 \cdot 0.5\text{H}_2\text{O}$	$2 \cdot \text{H}_2\text{O}$	$4 \cdot \text{H}_2\text{O}$	$5 \cdot 1.5\text{H}_2\text{O}$		$1 \cdot 0.5\text{H}_2\text{O}$	$2 \cdot \text{H}_2\text{O}$	$4 \cdot \text{H}_2\text{O}$	$5 \cdot 1.5\text{H}_2\text{O}$
Fe(1)-N(1)	1.96	1.97	1.98	1.94	N(1)Fe(1)N(8)	107.9	102.6	105.9	102.6
Fe(1)-N(3)	1.96	1.91	1.93	1.95	N(1)Fe(1)N(6)	95.3	92.5	95.1	100.1
Fe(1)-N(4)	1.95	1.97	1.98	1.93	N(1)Fe(1)N(9)	97.1	92.1	96.6	102.2
Fe(1)-N(6)	1.95	1.96	1.98	1.96	N(1)Fe(1)N(3)	75.2	79.8	75.6	85.3
Fe(1)-N(8)	1.86	1.88	1.90	1.86	N(3)Fe(1)N(9)	97.8	102.1	100.3	102.9
Fe(1)-N(9)	1.96	1.95	1.96	1.96	N(3)Fe(1)N(4)	75.8	81.2	80.6	73.7
$2\sigma^2 (\text{Fe-N}), \text{Å}^2$	0.014	0.013	0.013	0.012	F_i (*)	2.7	2.5	1.8	1.6

* The determination accuracy for parameters (interatomic distances and angles) based on the EXAFS data is $\pm 1\%$ (for the nearest sphere of the environment). $F_i = \sum_i^N w_i^2 (\chi_i^{\text{exp}}(k) - \chi_i^{\text{th}}(k))^2$, $w_i = \frac{k_i^n}{\sum_i^N k_i^n \sqrt{\chi_i^{\text{exp}}(k)}}$.

Table 2. Microstructure parameters for complex $[\text{FeL}_2](\text{ReO}_4)_2$ in the LS state obtained by single-scattering EXAFS data fitting.

Compound	Central Ion–Scattering Atom	N_i	$R_i, \text{Å}$	$2\sigma_i^2, \text{Å}^2$	F_i
$[\text{FeL}_2](\text{ReO}_4)_2$	Fe–N	6	1.96	0.010	2.7
	Fe–C	8	2.78	0.014	
	Fe–C	4	3.20		

Figure 3 illustrates a comparison of the experimental and simulated radial distribution function for $[\text{FeL}_2]\text{B}_{10}\text{H}_{10} \cdot \text{H}_2\text{O}$. The simulation was carried out using a multiple scattering approximation.

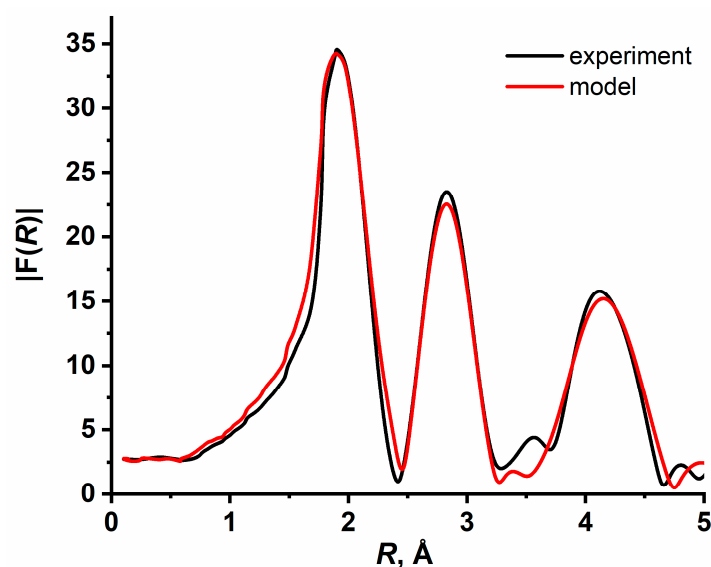


Figure 3. Comparison of the experimental and model radial distribution function for complex $[\text{FeL}_2]\text{B}_{10}\text{H}_{10}\cdot\text{H}_2\text{O}$.

Table 3 and Figures S5–S7 show the main vibration frequencies in the spectra of L and Fe(II) complexes. In the high-frequency spectral region for $1\cdot 0.5\text{H}_2\text{O}$, $2\cdot\text{H}_2\text{O}$, $4\cdot\text{H}_2\text{O}$, $5\cdot 1.5\text{H}_2\text{O}$, $\nu(\text{OH})$ vibrations are observed; in the wave number range of $3200\text{--}3050\text{ cm}^{-1}$ for all the complexes there are stretching vibrations of NH-groups, and in the range of $3100\text{--}2850\text{ cm}^{-1}$ there are vibrations of $\nu(\text{CH})$. In the wave number range of $1650\text{--}1450\text{ cm}^{-1}$, there are stretching and bending vibration bands inherent in heterocyclic rings. The spectra of the complexes in the range of ring vibrations exhibit a change in the number and position of the imidazole and pyridine bands in comparison with the spectrum of the ligand, which indicates the coordination of nitrogen atoms of the rings to Fe(II) ions. The presence of non-split bands inherent in stretching vibrations characteristic of the SO_4^{2-} and ReO_4^- anions indicates the fact that they are in outer-sphere position. The vibration bands of the B–H bonds of the outer-sphere anions $\text{B}_{10}\text{H}_{10}^{2-}$ and $\text{B}_{12}\text{H}_{12}^{2-}$ are centered at the wave numbers of 2470 cm^{-1} ($\nu(\text{BH})$) and 1075 cm^{-1} ($\delta(\text{BBH})$). In the case of the spectra for $4\cdot\text{H}_2\text{O}$, $5\cdot 1.5\text{H}_2\text{O}$ they are shifted with respect to those observed in the spectra of the initial salts, which could be, to all appearance, caused by the formation of $\text{H}_2\text{O}^{\delta-}\cdots\delta^+\text{H-B}$ bonds. In the far region of the spectra of all the complexes, Fe($3d^6$)–ligand(π) charge-transfer transition bands and vibration bands (M–N) are observed. The position of these bands is typical for the spectra of low-spin octahedral iron(II) complexes [35].

The diffuse reflectance spectra (DRS, Figures S8–S12) of all the obtained complexes exhibit intense metal-ligand charge transfer bands $\nu_1(e_g \rightarrow \pi_L^*)$ in the wavelength range of $300\text{--}350\text{ nm}$ ($\lambda_{\text{max}} \approx 324\text{--}326\text{ nm}$). The DRS of $4\cdot\text{H}_2\text{O}$ and $5\cdot 1.5\text{H}_2\text{O}$ exhibit three absorption bands, too, (see Table 4); they correspond to the ${}^1\text{A}_1 \rightarrow {}^1\text{T}_2$, ${}^1\text{A}_1 \rightarrow {}^1\text{T}_1$ and ${}^1\text{A}_1 \rightarrow {}^1\text{A}_2$ transitions in the strong octahedral field of the ligands. For low-spin axially distorted octahedral iron(II) complexes, the term ${}^1\text{T}_1$ is transformed according to the representation of ${}^1\text{E} + {}^1\text{A}_2$, whereas term ${}^1\text{T}_2$ is transformed according to the representation of ${}^1\text{E} + {}^1\text{B}_2$ [36]. Therefore, the ${}^1\text{A}_1 \rightarrow {}^1\text{B}_2$, ${}^1\text{A}_1 \rightarrow {}^1\text{A}_2$ and ${}^1\text{A}_1 \rightarrow {}^1\text{E}$ wide transition bands (see Table 4) observed in the spectra of $1\cdot 0.5\text{H}_2\text{O}$, $2\cdot\text{H}_2\text{O}$ and **3**, indicate the fact that an axial distortion of the octahedral coordination of these complexes occur. Low-intensity transitions and overlapping three wide bands do not make it possible to perform reliable quantitative calculations of crystal field parameters in this case. The spectra of all the complexes do not exhibit the ${}^5\text{T}_2 \rightarrow {}^5\text{E}$ band, which is caused by the HS state of iron(II). We were able to calculate the splitting parameters based on the difference between ${}^1\text{A}_1 \rightarrow {}^1\text{T}_2$ and ${}^1\text{A}_1 \rightarrow {}^1\text{T}_1$ absorption frequencies [36] for low-spin (LS) forms of complexes with *closo*-borate anions. The B values were computed using the formula $16B = [\nu({}^1\text{A}_1 \rightarrow {}^1\text{T}_2) - \nu({}^1\text{A}_1 \rightarrow {}^1\text{T}_1)]$. The

values C and Δ_{LS} (Table 4) were calculated using the equations: $\nu_{LS} = \Delta_{LS} - C + 86B^2/\Delta_{LS}$ and $C = 4.41 \cdot B$ [36–38]. The obtained data show that 2,6-bis(1*H*-imidazol-2-yl)pyridine is a strong field ligand. In addition, these data, as well as the values obtained for a number of previously synthesized Fe(II) complexes with 2,6-bis(benzimidazol-2-yl)pyridine and 2,6-bis(4,5-dimethyl-1*H*-imidazole) [22–24], obey the inequality that reflects the condition for the manifestation of SCO [37]: $19.000 \text{ cm}^{-1} \leq \Delta_{LS} \leq 22.000 \text{ cm}^{-1}$.

Table 3. The main vibrational frequencies (cm^{-1}) in the spectra of L and complexes.

L	1·0.5H ₂ O	2·H ₂ O	3	4·H ₂ O	5·1.5H ₂ O	Assignment
	3485	3433		3225	3269	$\nu(\text{OH})$
3100 _w	3020 _w	3147 3116	3050 _w	3151 3130	3148 3129	$\nu(\text{NH})$
3079 3035	3060 3021	3067	3067	2954 2924 2854	2988 2040 2849	$\nu(\text{CH})$
1598 1573 1552	1595 1570 1550	1569 1551 1479	1593 1566 1552	1622 1558 1490 1469	1622 1558 1490 1471	R _{ring}
	1118 1085 1070					$\nu(\text{SO}_4)$
			903			$\nu(\text{ReO}_4)$
				2473	2493	$\nu(\text{B-H})$
				1086 1036	1105 1054	$\delta(\text{BBH})$
	496	491	485	485	484	Fe(3d ⁶)–ligand (π) charge-transfer transition
	385 356 330	376 334	381 321	334	333	$\nu(\text{M-N})$

Table 4. Parameters of diffuse reflectance spectra.

Complex	$\lambda(^1A_1 \rightarrow ^1T_2)$	$\lambda(^1A_1 \rightarrow ^1B_2)$	$\lambda(^1A_1 \rightarrow ^1T_1)$	$\lambda(^1A_1 \rightarrow ^1A_2)$	$\lambda(^1A_1 \rightarrow ^1E)$	Calculated Parameter		
						B	C	Δ_{LS}
1·0.5H ₂ O		454		613	536			
2·H ₂ O		454		624	539			
3		432		603	503			
4·H ₂ O	475		518	620		109.3	482.0	1.97×10^4
5·1.5H ₂ O	465		518	620		137.5	606.5	1.98×10^4

The Mössbauer spectra of complexes 1·0.5H₂O, 2·H₂O, 3 and 5·1.5H₂O represent quadrupole doublets whose parameters correspond to the LS state of iron(II) (Figure 4). The spectrum of 4·H₂O also exhibits a broadened doublet related to the HS form of the complex (36%). The parameters of the Mössbauer spectra are presented in Table 5.

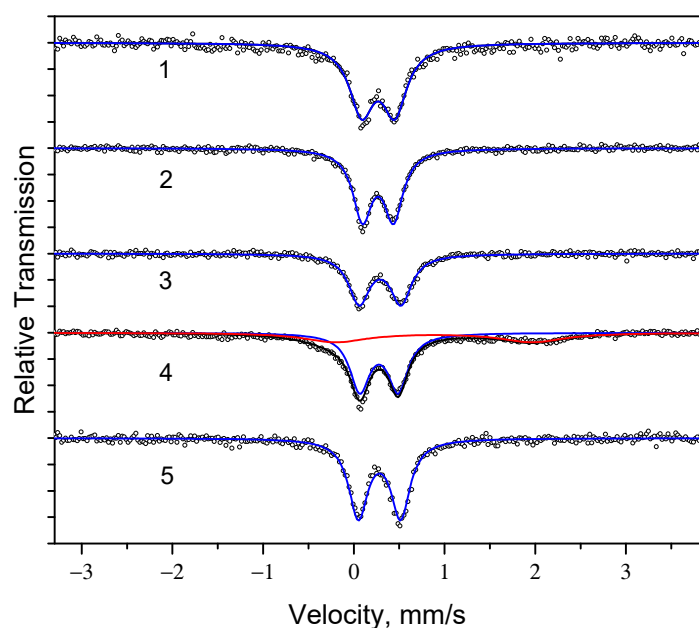


Figure 4. Mössbauer spectra of complexes **1**·0.5H₂O, **2**·H₂O, **3**, **4**·H₂O, **5**·1.5H₂O (1–5).

Table 5. Mössbauer spectra parameters of the complexes.

Complex	δ , mm/s	ϵ , mm/s	Γ , mm/s
1 ·0.5H ₂ O	0.269	0.364	0.33
2 ·H ₂ O	0.266	0.342	0.25
3	0.288	0.464	0.28
4 ·H ₂ O	0.278 (64%)	0.420	0.26
	0.925 (36%)	2.224	0.80
5 ·1.5H ₂ O	0.282	0.465	0.25

The temperature dependences of the effective magnetic moment for the analyzed complexes are shown in Figure 5. Spin crossover (SCO) is observed for all the compounds under investigation. In the case of complexes **1**·0.5H₂O, **2**·H₂O, **3** the μ_{eff} values observed in the thermal stability range (2.35, 2.1 and 3.35 μ_{B} , respectively), are significantly lower than the theoretical spin-only value of 4.9 μ_{B} for the Fe(II) ion. The **4**·H₂O and **5**·1.5H₂O complexes are more stable and thus a temperature of 600 K could be reached. For these compounds, a complete spin-crossover is observed. However, the μ_{eff} values observed in the HS state of these compounds are also lower than the theoretical value for Fe(II). It should be noted that the experimental μ_{eff} values for **4**·H₂O and **5**·1.5H₂O complexes are in the range of 4.6–5.7 observed for Fe(II) compounds [39,40]. In the case of **1**·0.5H₂O and **2**·H₂O the residual effective magnetic moment in LS state (0.65 and 0.4 μ_{B} , respectively), is presented by $\mu_{\text{eff}}(T)$ dependences. This fact could be connected with temperature-independent paramagnetism. Complexes **3**, **4**·H₂O and **5**·1.5H₂O in LS state exhibit diamagnetism with a zero μ_{eff} value. Despite the fact that low μ_{eff} values are achieved in the investigated temperature range for **1**·0.5H₂O and **3**, the condition of $d^2(\mu_{\text{eff}}(T))/dT^2 = 0$ could be satisfied and some values of SCO temperature could be determined. Table 6 shows the temperature values of direct ($T_{\text{c}\uparrow}$) and inverse ($T_{\text{c}\downarrow}$) transitions. For the [FeL₂]Br₂·H₂O one could suggest that the SCO temperature is higher than 420 K. The determined temperature of the inverse transition increases in a series of [FeL₂](ReO₄)₂ → [FeL₂]SO₄·0.5H₂O → [FeL₂]B₁₀H₁₀·H₂O → [FeL₂]B₁₂H₁₂·1.5H₂O.

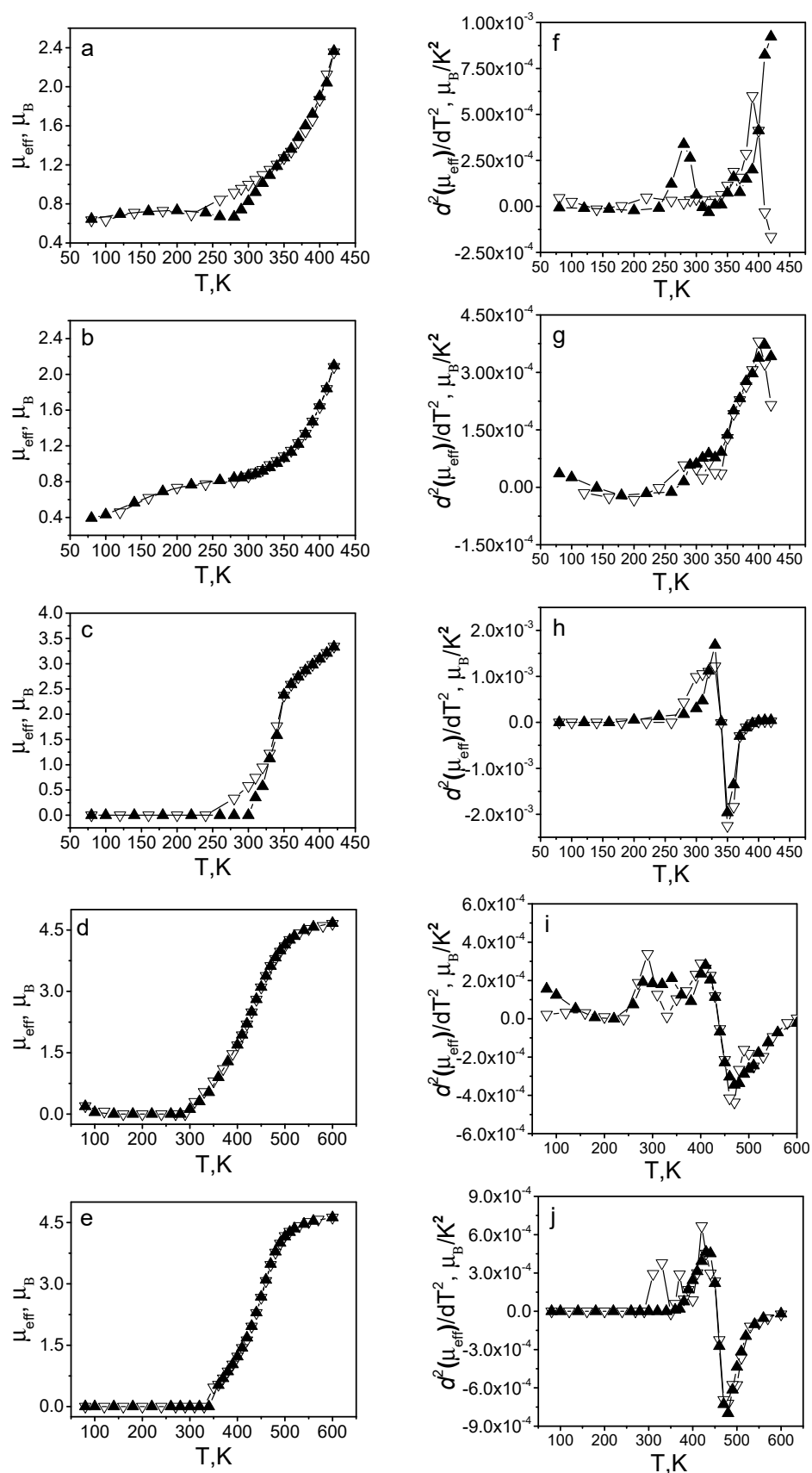


Figure 5. Dependences of $\mu_{\text{eff}}(T)$ (a–e) and $d^2(\mu_{\text{eff}}(T))/dT^2$ (f–j) for $1 \cdot 0.5\text{H}_2\text{O}$ (a,f), $2 \cdot \text{H}_2\text{O}$ (b,g), $3 \cdot \text{H}_2\text{O}$ (c,h), $4 \cdot \text{H}_2\text{O}$ (d,i), $5 \cdot 1.5\text{H}_2\text{O}$ (e,j). The white and black triangles in the figure correspond to the samples cooling and heating processes respectively.

Table 6. The temperatures of direct ($T_{c\uparrow}$) and inverse ($T_{c\downarrow}$) SCO for the studied complexes.

Complex	$T_{c\uparrow}$, K	$T_{c\downarrow}$, K
$[\text{FeL}_2]\text{SO}_4 \cdot 0.5\text{H}_2\text{O}$	>420	409
$[\text{FeL}_2]\text{Br}_2 \cdot \text{H}_2\text{O}$	>420	>420
$[\text{FeL}_2](\text{ReO}_4)_2$	340	340
$[\text{FeL}_2]\text{B}_{10}\text{H}_{10} \cdot \text{H}_2\text{O}$	436	436
$[\text{FeL}_2]\text{B}_{12}\text{H}_{12} \cdot 1.5\text{H}_2\text{O}$	455	455
$[\text{FeL}_2]\text{B}_{10}\text{H}_{10}$	447	440
$[\text{FeL}_2]\text{B}_{12}\text{H}_{12}$	458	458

The effect of the crystallization of water has been studied for $4 \cdot \text{H}_2\text{O}$ and $5 \cdot 1.5\text{H}_2\text{O}$ complexes (Figure 6). It should be noted that in the case of rarefied atmosphere the decomposition of the dehydrated complexes occurs in a lower temperature range than it is observed for initial compounds. Nevertheless, the SCO has been observed in this case, too. The μ_{eff} value of $4.65 \mu_{\text{B}}$ achieved in HS state for **4** corresponds to the value observed for the initial complex. In the case of **5** complex, the μ_{eff} value ($4.6 \mu_{\text{B}}$) exhibits an increase after dehydration. Residual μ_{eff} values ($\sim 1\text{--}1.5 \mu_{\text{B}}$) have been registered to occur for both complexes in the LS state. The SCO temperature increases after dehydration; however, the **5** complex demonstrates the highest SCO temperature values as it is observed in the case of the initial compound. Thus, the dehydration of $4 \cdot \text{H}_2\text{O}$ and $5 \cdot 1.5\text{H}_2\text{O}$ complexes lead to appearing residual μ_{eff} value and to an increase in the temperature of SCO.

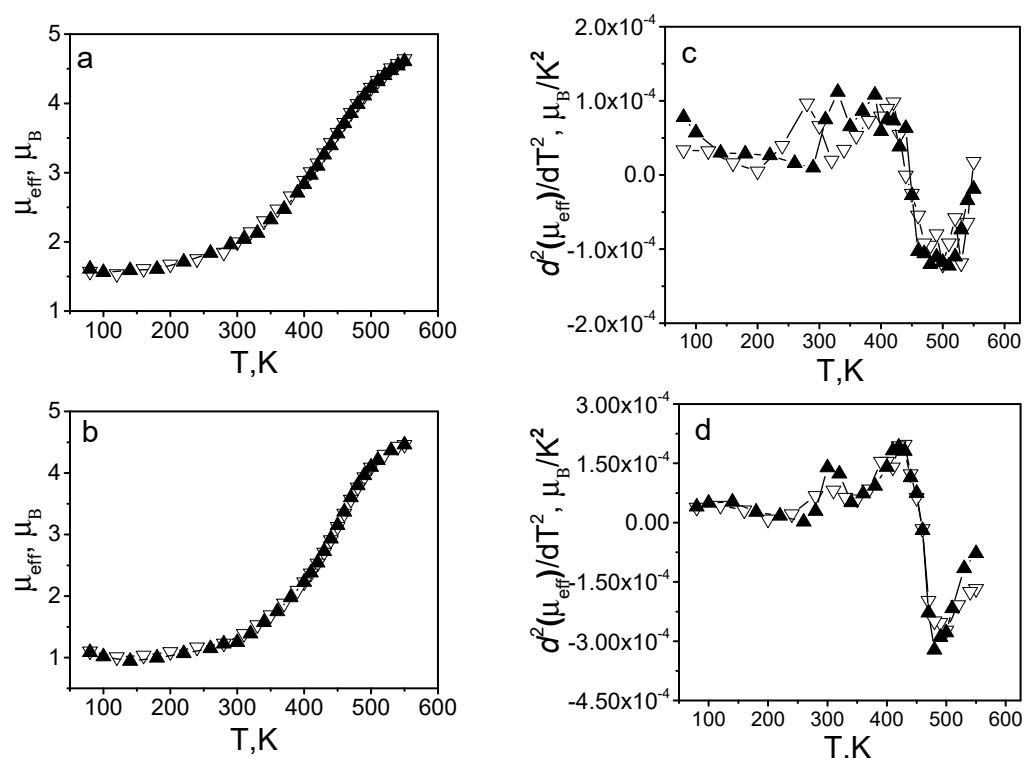


Figure 6. Dependences of $\mu_{\text{eff}}(T)$ (a,b) and $d^2(\mu_{\text{eff}}(T))/dT^2$ (c,d) for dehydrated complexes **4** (a,c), **5** (b,d). The white and black triangles in the figure correspond to the samples cooling and heating processes respectively.

4. Conclusions

In this work, we have synthesized and investigated five novel coordination compounds of various iron(II) salts with 2,6-bis(1*H*-imidazol-2-yl)pyridine (L). The structure of the coordination core of the complexes has been determined by means of EXAFS spectra simulation. Two ligand molecules are coordinated to the iron(II) ion in a tridentate-cyclic fashion by the nitrogen atom belonging to pyridine and two nitrogen atoms belonging to

imidazole rings. Thus, the complexes have the distorted-octahedral structure of the coordination polyhedron, the FeN₆ core. The studies on the $\mu_{\text{eff}}(T)$ dependence have shown that complexes having such a composition as [FeL₂]SO₄·0.5H₂O, [FeL₂]Br₂·H₂O, [FeL₂](ReO₄)₂, [FeL₂]B₁₀H₁₀·H₂O, [FeL₂]B₁₂H₁₂·1.5H₂O exhibit an ¹A₁ ↔ ⁵T₂ high-temperature spin crossover. A comparison of the data obtained for the synthesized compounds with those obtained by us earlier [21–24] shows that spin-crossover ¹A₁ ↔ ⁵T₂ is observed in all complexes of Fe(II) with 2,6-bis(imidazole-2-yl)pyridines. The temperatures of direct SCO, T_c↑, in most compounds are significantly higher than room temperature.

Supplementary Materials: The following supporting information can be downloaded at: <https://www.mdpi.com/article/10.3390/molecules27165093/s1>, Figure S1: NMR ¹H of 2,6-di(1H-imidazol-2-yl)pyridine, 100 MHz, NS 24; Figure S2: NMR ¹³C of 2,6-di(1H-imidazol-2-yl)pyridine, 100 MHz, NS 96; Figure S3: NMR ¹³C of 2,6-di(1H-imidazol-2-yl)pyridine, 100 MHz, NS 7376; Figure S4: NMR ¹³C of 2,6-di(1H-imidazol-2-yl)pyridine, 100 MHz, NS 176; Figure S5: IR spectrum of 2,6-bis(1H-imidazol-2-yl)pyridine (L); Figure S6: IR spectrum of [FeL₂]B₁₀H₁₀·H₂O (4·H₂O); Figure S7: IR spectrum of [FeL₂]B₁₂H₁₂·1.5H₂O (5·1.5H₂O); Figure S8: Comparison of the experimental DRS and model for complex [FeL₂]SO₄·0.5H₂O; Figure S9: Comparison of the experimental DRS and model for complex [FeL₂]Br₂·H₂O; Figure S10: Comparison of the experimental DRS and model for complex [FeL₂](ReO₄)₂; Figure S11: DRS for complex [FeL₂]B₁₀H₁₀·H₂O; Figure S12: DRS for complex [FeL₂]B₁₂H₁₂·1.5H₂O.

Author Contributions: Manuscript conception, writing and original draft preparation, data analysis and interpretation, L.G.L.; synthesis of the studied complexes, diffuse reflectance and IR spectroscopy, O.G.S.; studies of magnetic properties, E.V.K.; EXAFS spectroscopy, S.V.T.; synthesis of ligand, A.Y.T. and I.A.O.; Mössbauer spectroscopy methods, S.A.P.; synthesis of the *closo*-borates, data analysis, K.Y.Z.; editing, supervision, N.T.K. All authors have read and agreed to the published version of the manuscript.

Funding: This research work was partially supported by the Russian Science Foundation (grant No. 20-63-46026) and by the Ministry of Science and Higher Education of the Russian Federation (projects No. 121031700313-8, 121031700314-5, 121071500036-4, 1021051403061-8-1.4.1).

Institutional Review Board Statement: Not applicable.

Informed Consent Statement: Not applicable.

Data Availability Statement: The data presented in this study are available on request from the corresponding authors.

Acknowledgments: All the EXAFS procedures were performed at the Siberian Synchrotron and Terahertz Radiation Center of the Novosibirsk VEPP-3 complex at Budker Institute of Nuclear Physics of the SB RAS (Novosibirsk, Russia). The authors thank V.V. Kriventsov for his assistance in XAS measurements. Authors would like to acknowledge the Multi Access Chemical Research Center SB RAS for spectral and analytical measurements.

Conflicts of Interest: The authors declare no conflict of interest.

Sample Availability: Samples of the compounds are available from the authors on request.

References

1. Gutlich, P.; Goodwin, H. *Spin Crossover in Transition Metal Compounds I–III*; Springer: Berlin/Heidelberg, Germany, 2004; pp. 233–235.
2. Halcrow, M.A. *Spin-Crossover Materials Properties and Applications*; John Wiley & Sons Ltd.: Chichester, UK, 2013; p. 562.
3. Shatruk, M.; Phan, H.; Chrisostomo, B.A.; Suleimenova, A. Symmetry-breaking structural phase transitions in spin crossover complexes. *Coord. Chem. Rev.* **2015**, *289–290*, 62–73. [[CrossRef](#)]
4. Feltham, H.L.C.; Barltrop, A.S.; Brooker, S. Spin crossover in iron(II) complexes of 3,4,5-tri-substituted-1,2,4-triazole (Rdpt), 3,5-di-substituted-1,2,4-triazolate (dpt[−]), and related ligands. *Coord. Chem. Rev.* **2017**, *344*, 26–53. [[CrossRef](#)]
5. Scott, H.S.; Staniland, R.W.; Kruger, P.E. Spin crossover in homoleptic Fe(II) imidazolylimine complexes. *Coord. Chem. Rev.* **2018**, *362*, 24–43. [[CrossRef](#)]
6. Kumar, K.S.; Ruben, M. Emerging trends in spin crossover (SCO) based functional materials and devices. *Coord. Chem. Rev.* **2017**, *346*, 176–205. [[CrossRef](#)]

7. Lavrenova, L.G. Spin crossover in homo- and heteroligand iron(II) complexes with tris(pyrazol-1-yl)methane derivatives. *Rus. Chem. Bull.* **2018**, *67*, 1142–1152. [CrossRef]
8. Shakirova, O.G.; Lavrenova, L.G. Spin crossover in new iron(II) coordination compounds with tris(pyrazol-1-yl)methane. *Crystals* **2020**, *10*, 843. [CrossRef]
9. Kahn, O.; Krober, J.; Jay, C. Spin transition molecular materials for displays and data recording. *Adv. Mater.* **1992**, *4*, 718–728. [CrossRef]
10. Gamez, P.; Costa, J.S.; Quesada, M.; Aromí, G. Iron Spin-Crossover compounds: From fundamental studies to practical applications. *Dalton Trans.* **2009**, 7845–7853. [CrossRef] [PubMed]
11. Hayami, S.; Holmes, S.M.; Halcrow, M.A. Spin-state switches in molecular materials chemistry. *J. Mater. Chem. C* **2015**, *3*, 7775–7778. [CrossRef]
12. Kumar, K.S.; Bayeh, Y.; Gebretsadik, T.; Elemo, F.; Gebrezgiabher, M.; Thomas, M.; Ruben, M. Spin-crossover in iron(II)-Schiff base complexes. *Dalton Trans.* **2019**, *48*, 15321–15377. [CrossRef] [PubMed]
13. Halcrow, M.A. Manipulating metal spin states for biomimetic, catalytic and molecular materials chemistry. *Dalton Trans.* **2020**, *49*, 15560–15567. [CrossRef] [PubMed]
14. Letard, J.-F.; Daro, N.; Aymonier, C.; Cansell, F.; Saint-Martin, S. Nouveau Materiau a Transition de spin, son Procédé de Preparation. European Patent 2391631, 7 December 2011.
15. Bousseksou, A.; Vieu, C.; Letard, J.-F.; Demont, P.; Tuchagues, J.-P.; Malaquin, L.; Menegotto, J.; Salmon, L. Molecular Memory and Method for Making Same. European Patent 1430552, 2004. Available online: <https://data.epo.org/gpi/EP1430552A1-MOLECULAR-MEMORY-AND-METHOD-FOR-MAKING-SAME> (accessed on 28 June 2022).
16. Piedrahita-Bello, M.; Angulo-Cervera, J.E.; Courson, R.; Molnár, G.; Malaquin, L.; Thibault, C.; Tondu, B.; Salmon, L.; Bousseksou, A. 4D printing with spin-crossover polymer composites. *J. Mater. Chem. C* **2020**, *8*, 6001–6005. [CrossRef]
17. Nguyen, T.D.; Veauthier, J.M.; Angles-Tamayo, G.F.; Chavez, D.E.; Lapsheva, E.L.; Myers, T.W.; Nelson, T.R.; Schelter, E.J. Correlating mechanical sensitivity with spin transition in the explosive spin crossover complex [Fe(Htrz)₃]_n[ClO₄]_{2n}. *J. Am. Chem. Soc.* **2020**, *142*, 4842–4851. [CrossRef] [PubMed]
18. Yuan, J.; Wu, S.Q.; Liu, M.J.; Sato, O.; Kou, H.Z. Rhodamine 6G-labeled pyridyl aroylhydrazone Fe(II) complex exhibiting synergetic spin crossover and fluorescence. *J. Am. Chem. Soc.* **2018**, *140*, 9426–9433. [CrossRef] [PubMed]
19. Benaicha, B.; Van Do, K.; Yangui, A.; Pittala, N.; Lussion, A.; Sy, M.; Bouchez, G.; Fourati, H.; Gomez-Garcia, C.J.; Triki, S.; et al. Interplay between spin-crossover and luminescence in a multifunctional single crystal iron(II) complex: Towards a new generation of molecular sensors. *Chem. Sci.* **2019**, *10*, 6791–6798. [CrossRef]
20. Boča, M.; Jameson, R.F.; Linert, W. Fascinating variability in the chemistry and properties of 2,6-bis-(benzimidazol-2-yl)-pyridine and 2,6-bis-(benzthiazol-2-yl)-pyridine and their complexes. *Coord. Chem. Rev.* **2011**, *255*, 290–317. [CrossRef]
21. Lavrenova, L.G.; Dyukova, I.I.; Korotaev, E.V.; Sheludyakova, L.A.; Varnek, V.A. Spin crossover in new iron(II) complexes with 2,6-bis(benzimidazole-2-yl)pyridine. *Rus. J. Inorg. Chem.* **2020**, *65*, 30–35. [CrossRef]
22. Ivanova, A.D.; Korotaev, E.V.; Komarov, V.Y.; Sheludyakova, L.A.; Varnek, V.A.; Lavrenova, L.G. Spin-crossover in iron(ii) coordination compounds with 2,6-bis(benzimidazol-2-yl)pyridine. *New J. Chem.* **2020**, *44*, 5834–5840. [CrossRef]
23. Ivanova, A.D.; Lavrenova, L.G.; Korotaev, E.V.; Trubina, S.V.; Sheludyakova, L.A.; Petrov, S.A.; Zhizhin, K.Y.; Kuznetsov, N.T. High-temperature spin crossover in complexes of iron(II) *closo*-borates with 2,6-bis(benzimidazol-2-yl)pyridine. *Russ. J. Inorg. Chem.* **2020**, *65*, 1687–1694. [CrossRef]
24. Ivanova, A.D.; Korotaev, E.V.; Komarov, V.Y.; Sukhikh, T.S.; Trubina, S.V.; Sheludyakova, L.A.; Petrov, S.A.; Tikhonov, A.Y.; Lavrenova, L.G. Spin crossover in iron(II) complexes with new ligand 2,6-bis(4,5-dimethyl-1H-imidazole-2-yl)pyridine. *Inorg. Chim. Acta* **2022**, *532*, 120746. [CrossRef]
25. Stupka, G.; Gremaud, L.; Bernardinelli, G.; Williams, A.F. Redox state switching of transition metals by deprotonation of the tridentate ligand 2,6-bis(imidazol-2-yl)pyridine. *Dalton Trans.* **2004**, 407–412. [CrossRef]
26. Hammes, B.S.; Damiano, B.J.; Tobash, P.H.; Hidalgo, M.J.; Yap, G.P.A. Tuning the redox properties of a 1-D supramolecular array via selective deprotonation of coordinated imidazoles around a Mn(II) center. *Inorg. Chem. Commun.* **2005**, *8*, 513–516. [CrossRef]
27. Arruda, E.G.R.; Farias, M.A.; Jannuzzi, S.A.V.; Almeida Gonsales, S.; Timm, R.A.; Sharma, S.; Zoppellaro, G.; Kubota, L.T.; Knobel, M.; Formiga, A.L.B. Synthesis, structural and magnetic characterization of a copper(II) complex of 2,6-di(1H-imidazol-2-yl)pyridine and its application in copper-mediated polymerization catalysis. *Inorg. Chim. Acta* **2017**, *466*, 456–463. [CrossRef]
28. Ren, C.-X.; Li, S.-Y.; Yin, Z.-Z.; Lu, X.; Ding, Y.-Q. [2,6-Bis(4,5-dihydro-1H-imidazol-2-yl)pyridine]dichloridomanganese(II). *Acta Cryst. E* **2009**, *65*, m572–m573. [CrossRef]
29. Shang, S.-M.; Ren, C.-X.; Wang, X.; Lu, L.-D.; Yang, X.-J. Bis[2,6-bis(4,5-dihydro-1H-imidazol-2-yl)pyridine]manganese(II) bis-(per-chlorate) acetonitrile solvate. *Acta Cryst. E* **2009**, *65*, m1023–m1024. [CrossRef]
30. Voss, M.E.; Beer, C.M.; Mitchell, S.A.; Blomgren, P.A.; Zhichkin, P.E. A simple and convenient one-pot method for the preparation of heteroaryl-2-imidazoles from nitriles. *Tetrahedron* **2008**, *64*, 645–651. [CrossRef]
31. Miller, H.C.; Muetterties, E.L.; Boone, J.L.; Garrett, P.; Hawthorne, M.F. Borane anions. *Inorg. Synth.* **1967**, *10*, 81–91. [CrossRef]
32. Piminov, P.A.; Baranov, G.N.; Bogomyagkov, A.V.; Berkaev, D.E.; Borin, V.M.; Dorokhov, V.L.; Karnaev, S.E.; Kiselev, V.A.; Levicev, E.B.; Meshkov, O.I.; et al. Synchrotron radiation research and application at VEPP-4. *Phys. Procedia* **2016**, *84*, 19–26. [CrossRef]
33. Klementev, K.V. Extraction of the fine structure from x-ray absorption spectra. *J. Phys. D Appl. Phys.* **2001**, *34*, 209. [CrossRef]

34. Gurman, S.J.; Binsted, N.; Ross, I. A rapid, exact curved-wave theory for EXAFS calculations. *J. Phys. C Solid State Phys.* **1984**, *17*, 143–151. [[CrossRef](#)]
35. Nakamoto, K. *Infrared and Raman Spectra of Inorganic and Coordination Compounds*; John Wiley & Sons Inc.: New York, NY, USA, 1986.
36. Lever, A.B.P. *Inorganic Electronic Spectroscopy*, 2nd ed.; Elsevier: Amsterdam, The Netherlands, 1985; ISBN 978-0-444-42389-4.
37. Hauser, A. *Ligand Field Theoretical Considerations. Spin Crossover in Transition Metal Compounds I*; Springer: Berlin/Heidelberg, Germany, 2004; Volume 233, pp. 49–58. [[CrossRef](#)]
38. Sugano, S.; Tanabe, Y.; Kamimura, H. *Multiplets of Transition—Metal ions in Crystals*; Academic Press: New York, NY, USA; Pure and Applied Physics: London, UK, 1970.
39. Selwood, P.W. *Magnetochemistry*; Interscience Publishers: New York, NY, USA, 1956.
40. Rakitin, Y.V.; Kalinnikov, V.T. *Modern Magnetochemistry*; Nauka: St. Petersburg, Russia, 1994.